Electronic Supplementary Material (ESI) for Journal of Materials Chemistry A.

Relieving hydrogen evolution and anodic corrosion of aqueous aluminum batteries with hybrid electrolytes

Xuejin Li, ‡ [a,b] Yongchao Tang, ‡ [b] Chuan Li[c], Haiming Lv, [b] Haodong Fan,[a] Wenlong Wang,[b] Tonghui Cai,[a] Yongpeng Cui,[a] Wei Xing,[a] Zifeng Yan,[a] Chunyi Zhi[b, c], Hongfei Li*[b]*

‡ These authors contributed equally to this work.

[a] State Key Laboratory of Heavy Oil Processing, China University of Petroleum, Qingdao 266580, China

[b] Songshan Lake Materials Laboratory, Dongguan, Guangdong 523808, China;

[c] Department of Materials Science and Engineering, City University of Hong Kong, 83 Tat Chee Avenue, Kowloon, Hong Kong 999077, China

Email: Dr. Hongfei Li, lihf@sslab.org.cn

Prof. Chunyi Zhi, cy.zhi@cityu.edu.hk

Experimental section

Materials Synthesis: All reagents were analytic grade, commercially available and used without further treatment. The potassium vanadate was synthesized by a hydrothermal reaction as reported in the literature.[1] Typically, 0.182 g V_2O_5 powder, 0.249 g KI, and 2.24 g KCl were dissolved in 30 mL deionized water. After being stirred for 30 min under room temperature, the solution was transferred into 50 mL autoclave and heated at 200 °C for 24 h. Afterward, the autoclave was cooled naturally to room temperature and the precipitate was collected by centrifugation. The product was washed with deionized water for three times and dried at 80 °C overnight. The as-prepared sample was denoted as KVO.

The aqueous electrolytes were prepared by dissolving various amounts of $AlCl_3$ (0.24, 0.6, 1.2, 1.8, and 2.4 g) and LiTFSI (24.4, 17.5, 12.1, 9.1, and 7.6 g, correspondingly) into 5 mL deionized water. The molar ratio of $AlCl_3$ to LiTFSI was calculated to be 0.2: 17, 0.5: 12, 1: 9, 1.5: 6.3, and 2: 5.3 respectively. Besides, 1 M

$AlCl_3$, 1 M $Al(NO_3)_3$, 1 M $Al_2(SO_4)_3$, 1 M $Al(OTF)_3$, and 5 M $Al(OTF)_3$ were also prepared by dissolving corresponding salts in deionized water.

Characterizations: The samples were characterized by X-ray diffraction (XRD, Rigaku MiniFlex 600 with Cu Kα radiation, λ=1.5406 Å), scanning electron microscopy (SEM, S-4800Hitachi) and transmission electron microscopy (TEM, JEM-2100 JEOL) for structure and morphology detection. X-ray photoelectron spectroscopy (XPS) was used to assess the surface composition and chemical state of the samples. The XPS measurements were carried out on the PHI-5000 Versa Probe spectrometer equipped with monochromatized Al-Kα radiation (1486.6 eV). Raman spectra were acquired with a Raman spectrometer (Labram ARAMIS).

Electrochemical Measurements: The KVO cathode was prepared by mixing KVO powder, Ketjen Black, and polyvinylidene fluoride in a weight ratio of 75:15:10 in N-methyl pyrrolidone to produce a slurry, which was then coated on graphite paper. The cathode was further dried at 60 ^oC for 4 h. The batteries were assembled using the as-prepared cathode and Al plate as anode in electrolytic cells. The batteries were tested using Land instrument and CHI electrochemical workstation. The three-electrode system tests were performed using Ag/AgCl as the reference electrode and Pt plate as the counter electrode.

Molecular dynamic (MD) simulations: MD simulations were performed using Forcite code embedded in the Material Studio program package. The interatomic interactions were described by the force field of a condensed-phase optimized molecular potential for atomisticsimulation studies (COMPASS). The van der Waals interactions were calculated within a cutoff distance of 12.5 Å, and the Ewald sum technique was used to calculate the electrostatic interaction. The canonical (NVT) ensemble was employed for the simulations. The temperature (298 K) of the system was controlled by the Andersen thermostat method. The total simulation time is 10 ns with the time step fixed at 1 fs, and data was collected at every 1 ps.

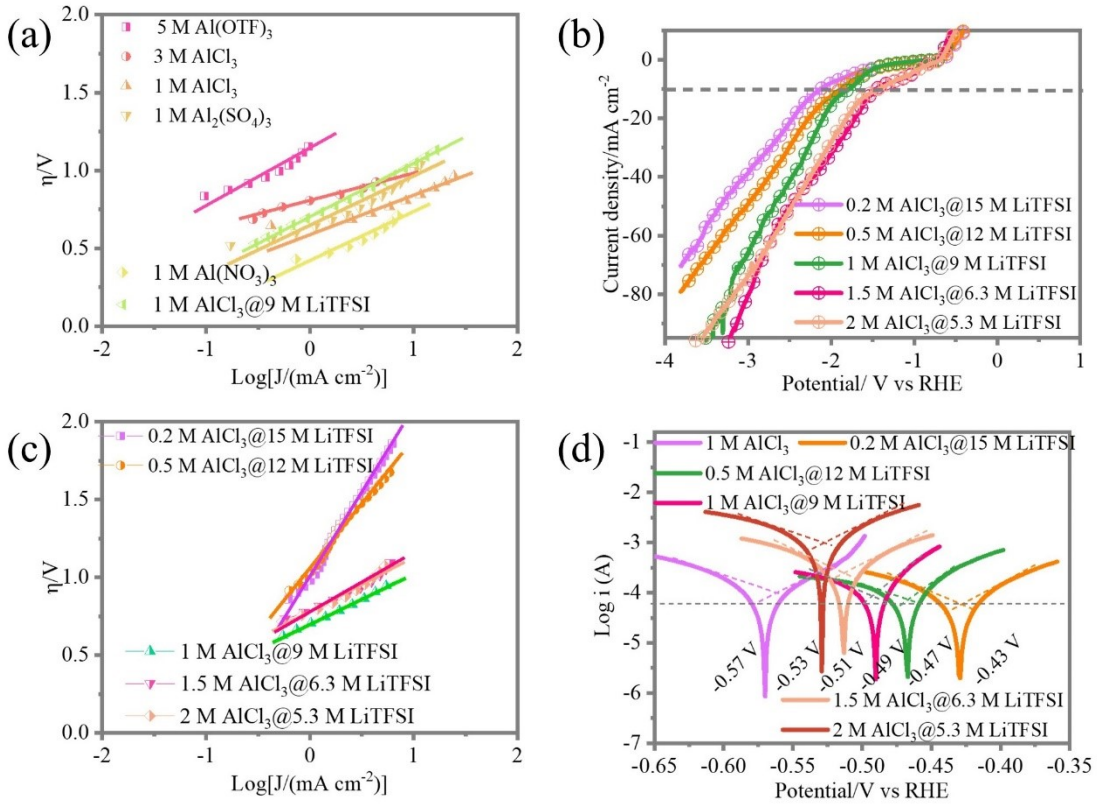

Figure S1 (a)Tafel curves of Al plate in various electrolytes; (b) LSV curves of Al plate in various electrolytes; (c) Tafel plots of Al plate in electrolytes with various LiTFSI concentrations; and (d) Tafel plots of Al plate in various saturated electrolytes.

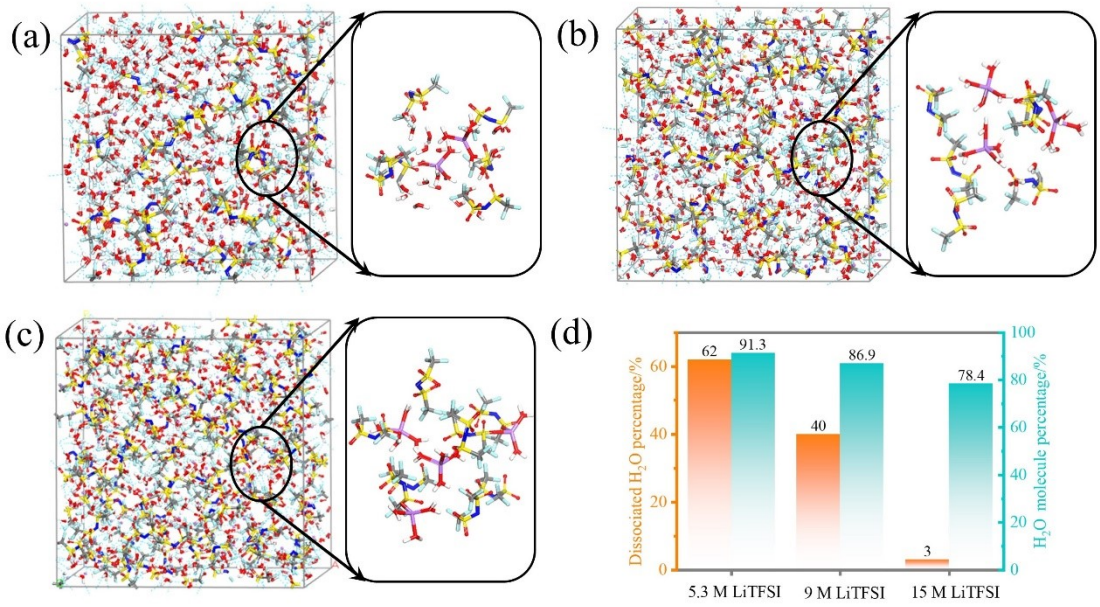

Figure S2 MD simulations of aqueous electrolytes. Snapshots of the local structures of (a) 5.3 M LiTFSI electrolyte, (b) 9 M LiTFSI electrolyte, and (c) 15 M LiTFSI

electrolyte; (d) the dissociated H_2O percentage and total H_2O percentage for three electrolytes at 10 ns.

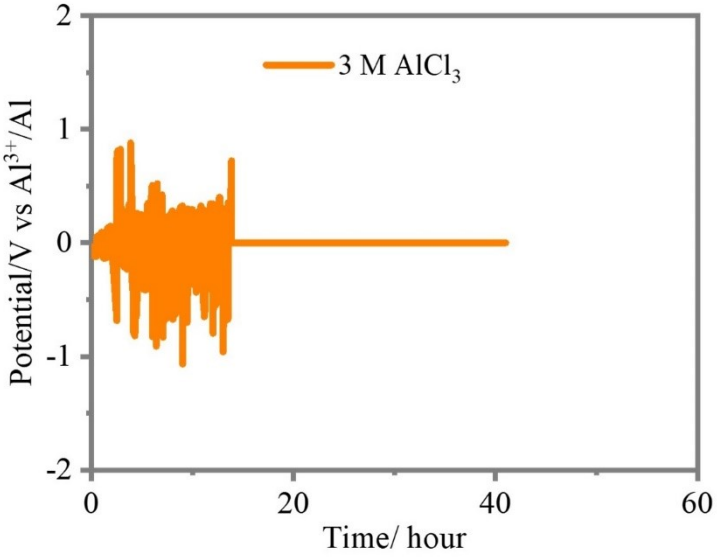

Figure S3 The tests of symmetric Al batteries with 3 M $AlCl_3$ electrolyte.

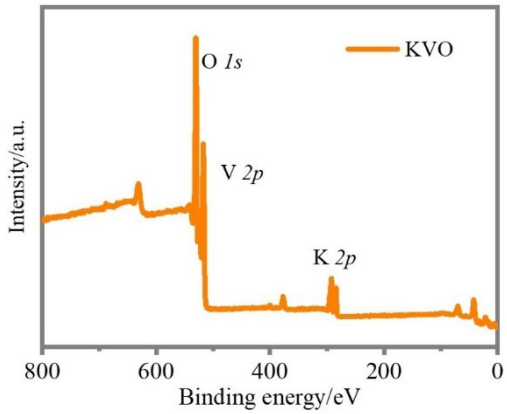

Figure S4 XPS spectrum of KVO.

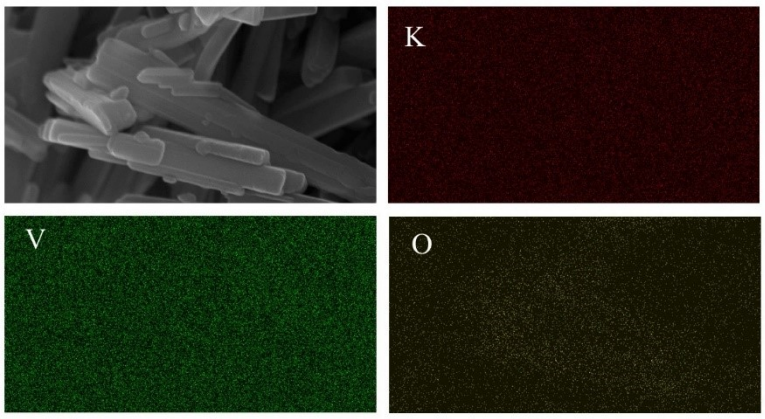

Figure S5 EDS elemental mapping of KVO.

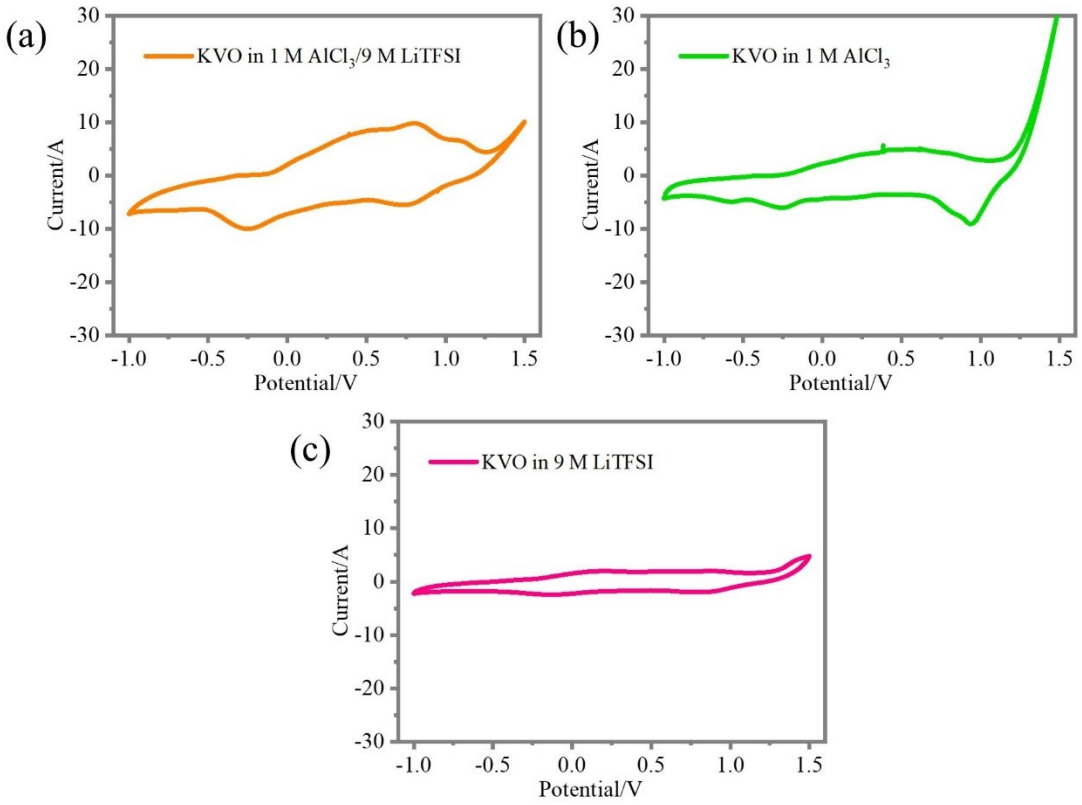

Figure S6 CV curves of KVO in various electrolytes.

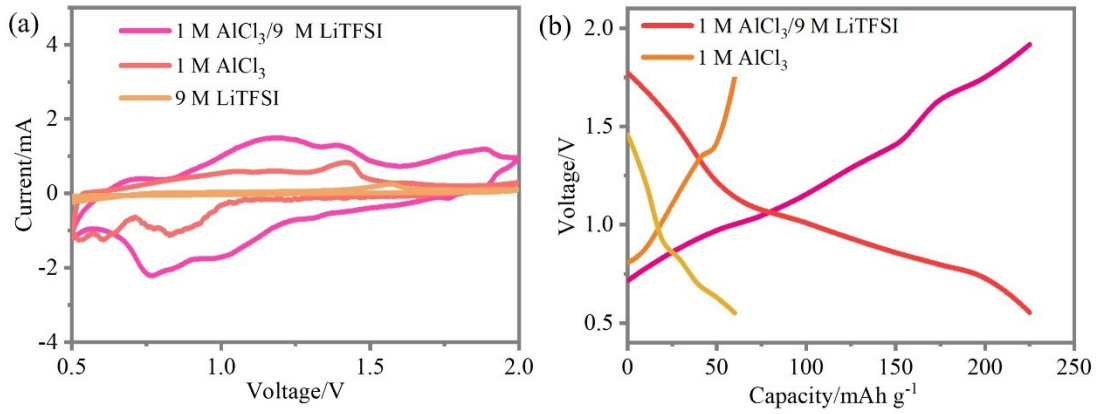

Figure S7 CV curves and charging-discharging curves of KVO//Al full battery in various electrolytes.

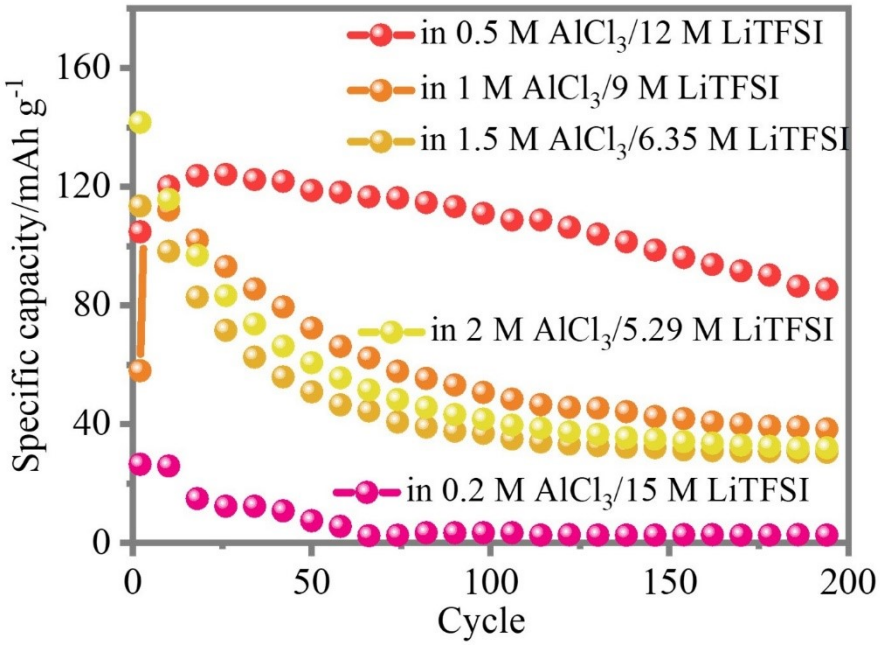

Figure S8 Cycling stability of KVO//Al plates in aqueous electrolytes with different LiTFSI concentrations.

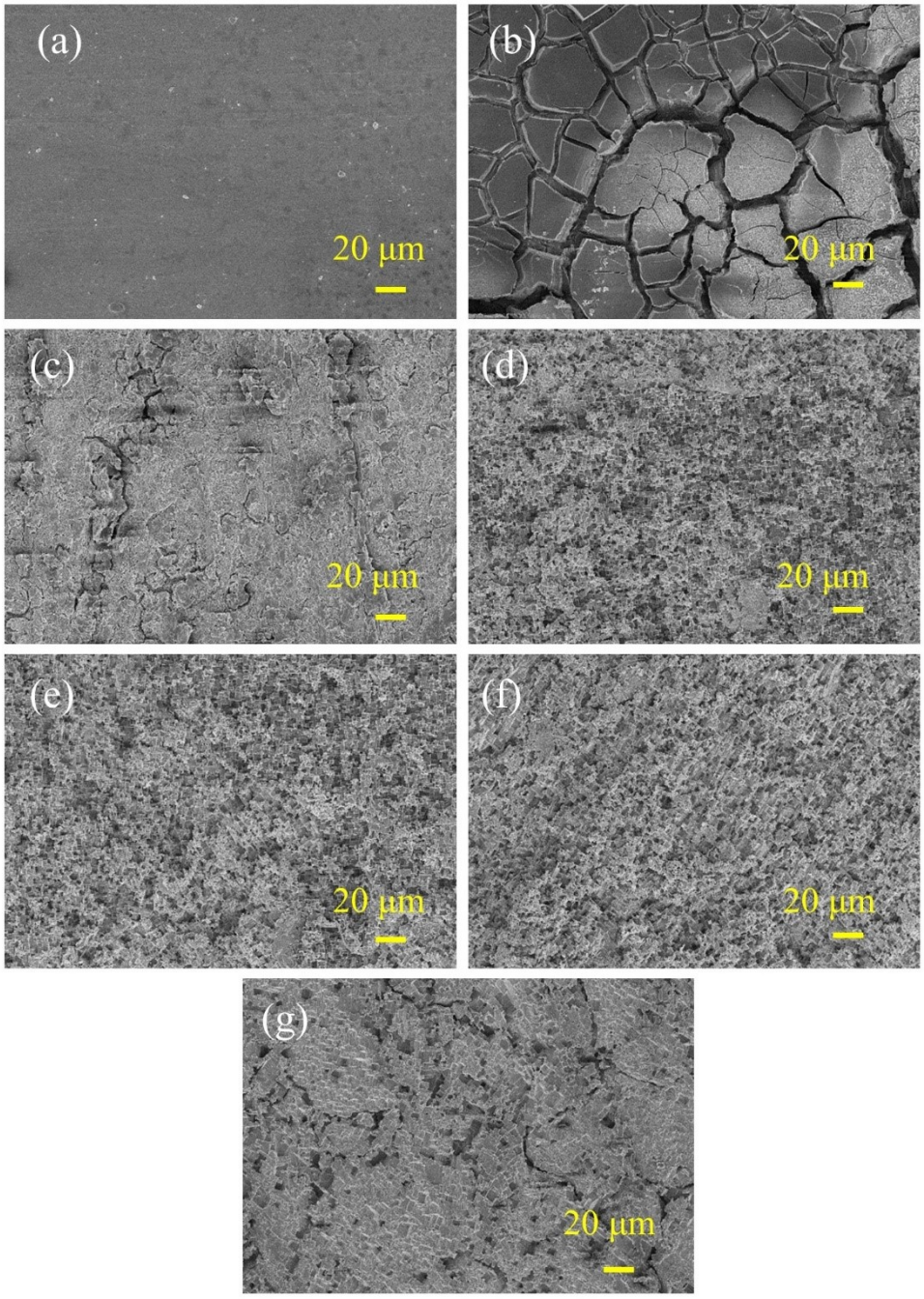

Figure S9 SEM images of Al plate after 300 cycles in (a) 1 M $AlCl_3$, (b) 0.2 M $AlCl_3$@15 M LiTFSI, (c) 0.5 M $AlCl_3$@12 M LiTFSI, (d) 1 M $AlCl_3$@9 M LiTFSI, (e) 1.5 M $AlCl_3$@6.35 M LiTFSI and (g) 2 M $AlCl_3$@5.29 M LiTFSI.

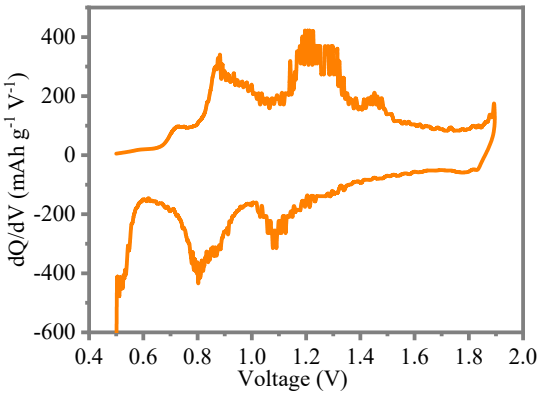

Figure S10 The differential capacity (dQ/dV) curve of the full Al//KVO battery at 1 A g^{-1}.

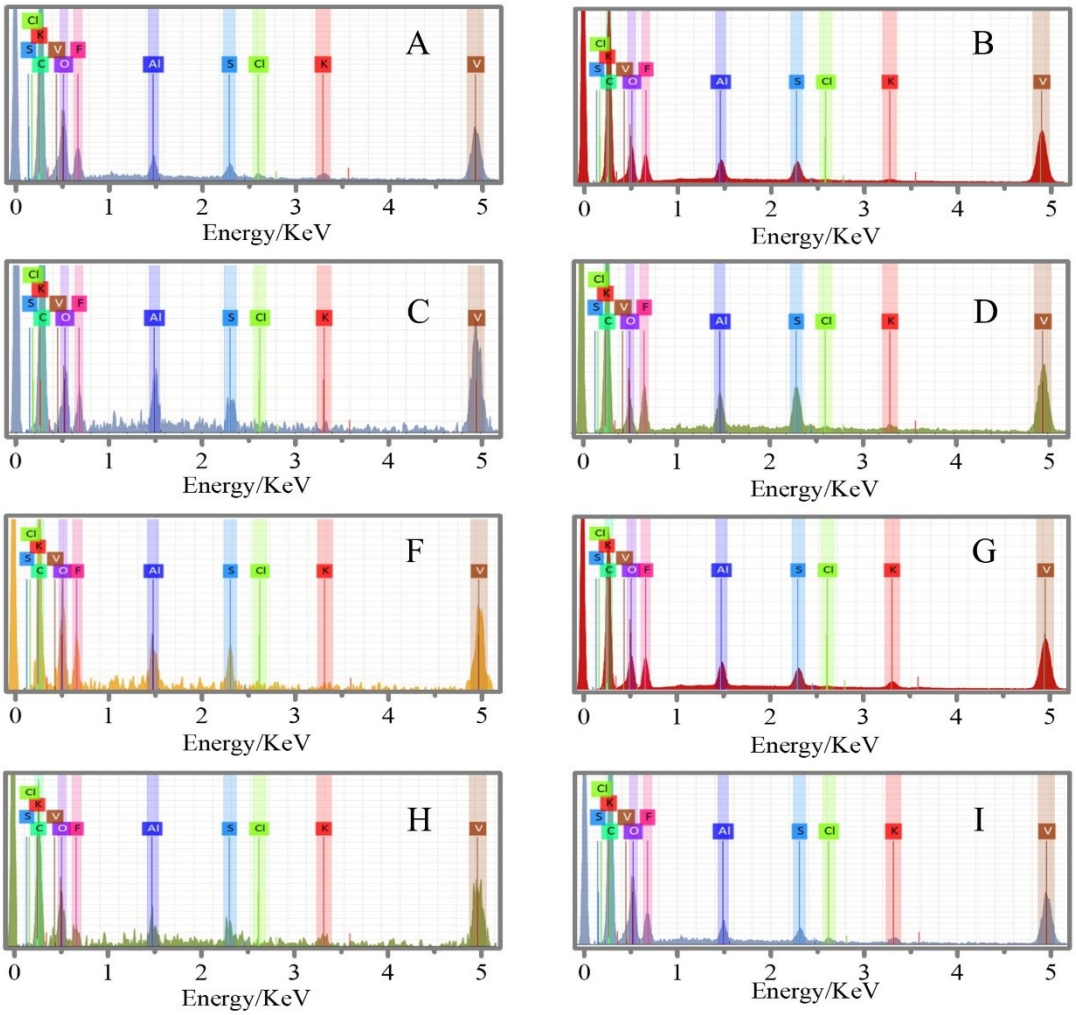

Figure S11 EDS of KVO under different charging/discharging states.

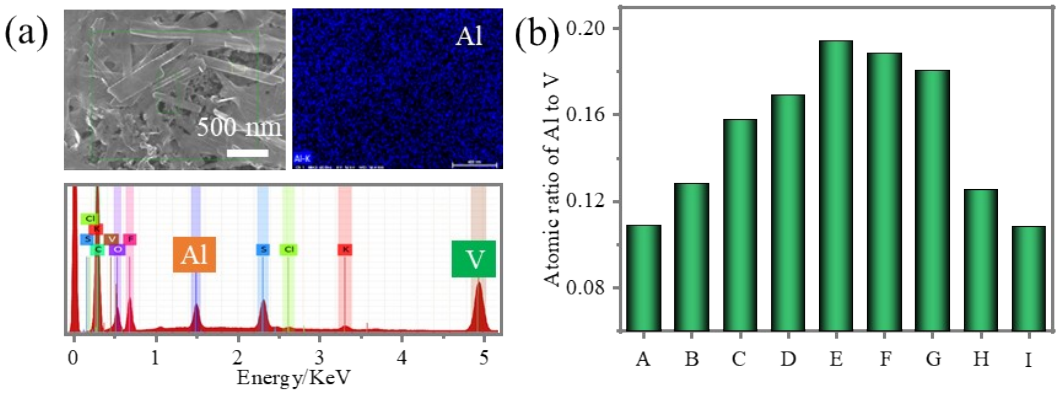

Figure S12 (a) Al mapping and EDS of KVO after fully discharge; (b) atom ratios of Al to V of KVO

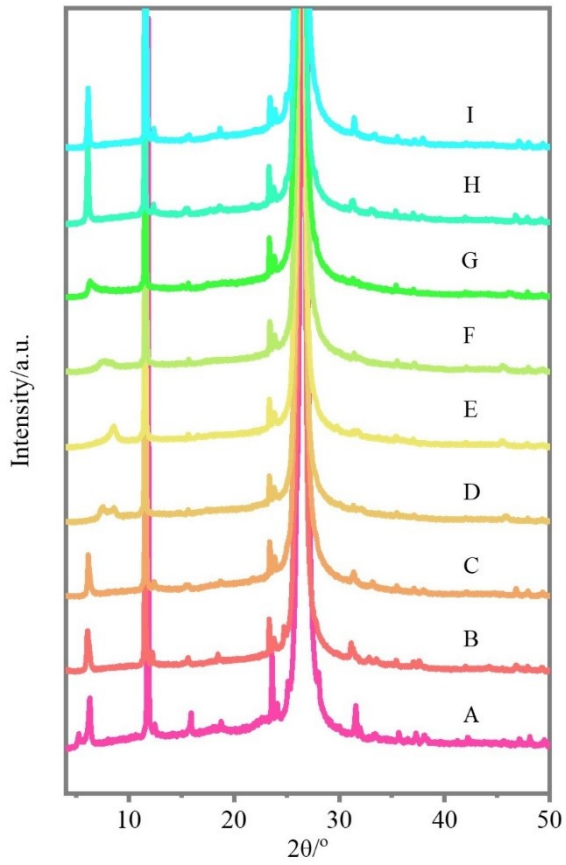

Figure S13 XRD patterns of KVO cathode under different charging/discharging states.

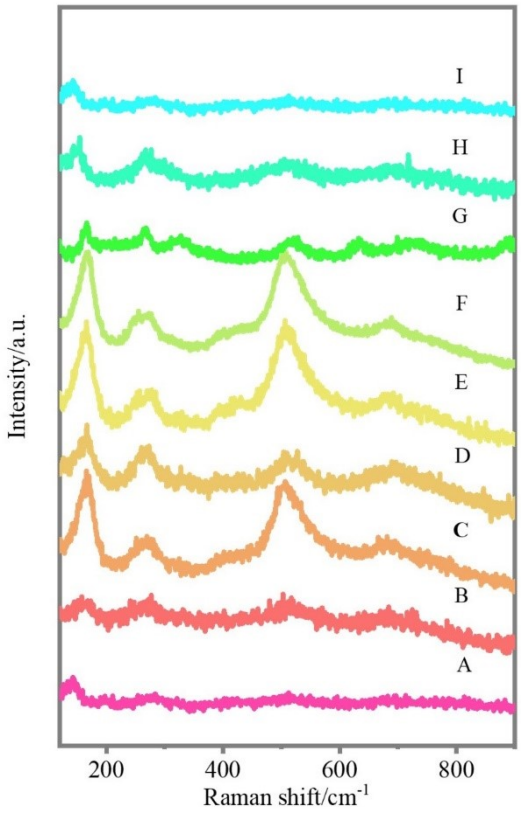

Figure S14 Ex-situ Raman spectra of KVO under different charging/discharging states.

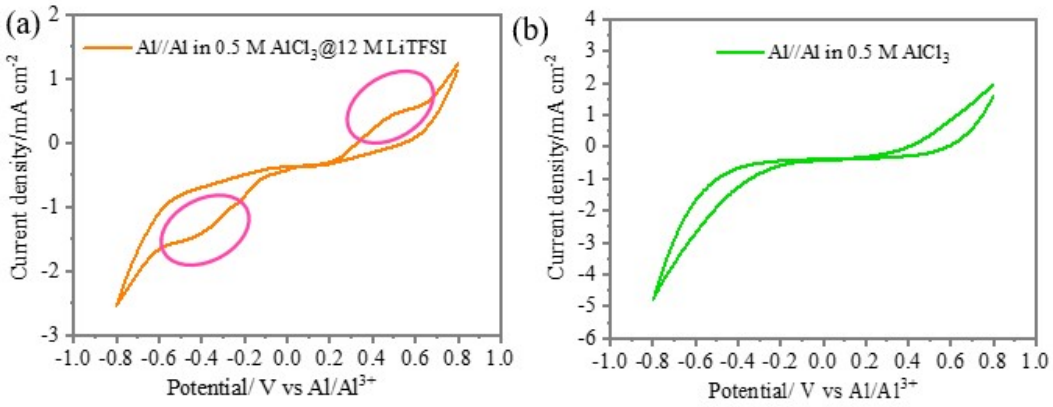

Figure S15 CV curves of Al//Al batteries with 0.5 M $AlCl_3$/12 M LiTFSI and 0.5 M $AlCl_3$ as electrolytes.

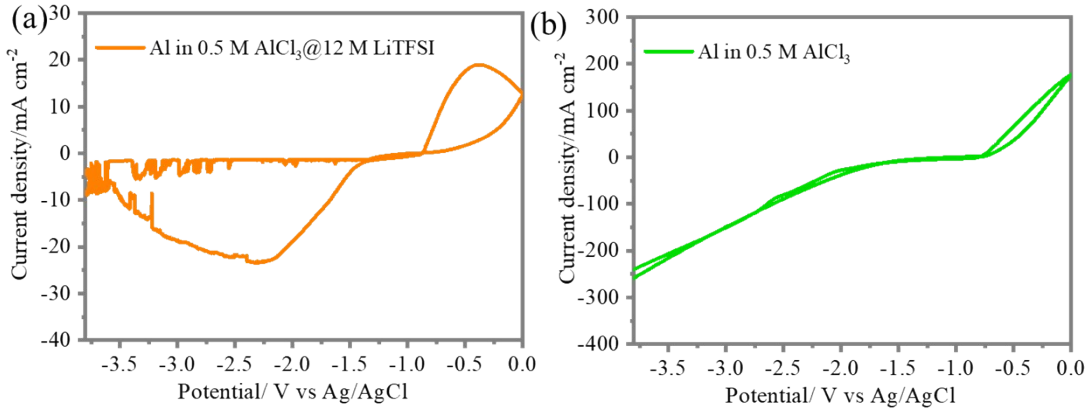

Figure S16 CV curves of Al in different electrolytes measured with a three-electrode system.

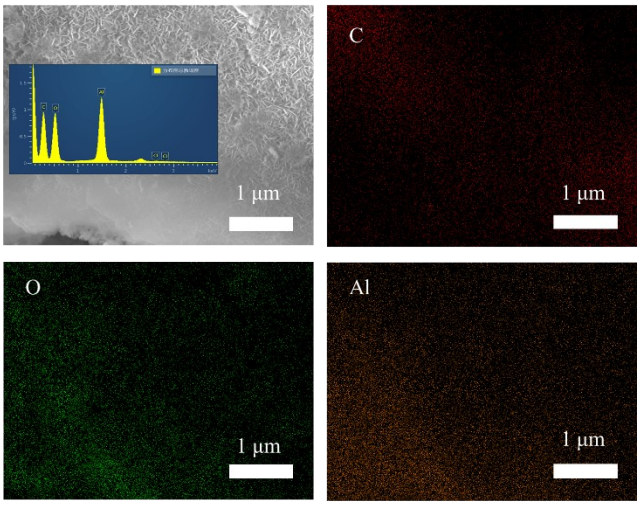

Figure S17 SEM image of graphite paper after discharging on graphite paper//Al battery and corresponding elemental mapping distributions

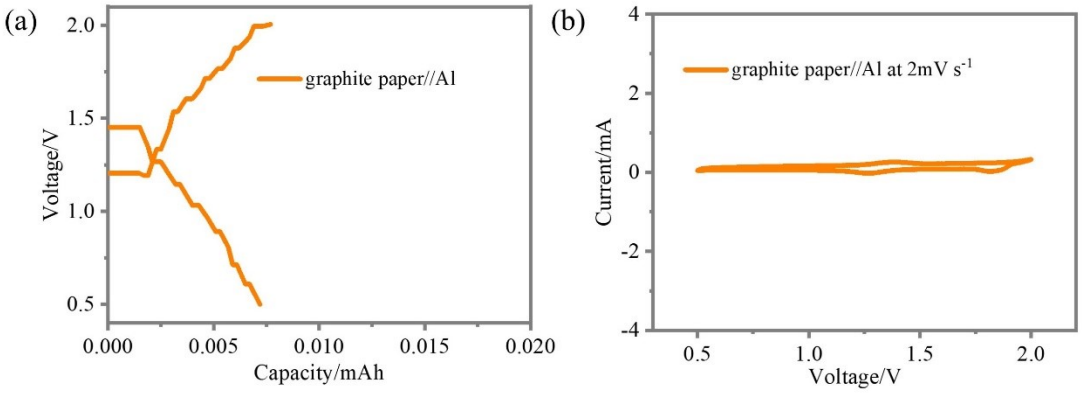

Figure S18 GCD profile and CV curve of graphite paper//Al battery.

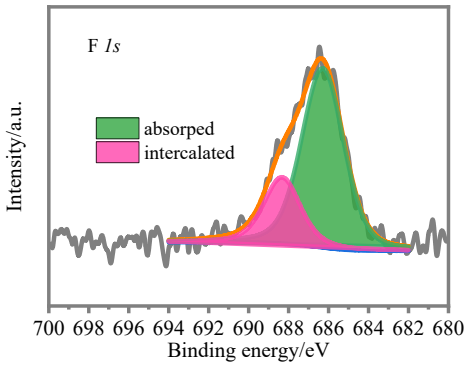

Figure S19 F 1s spectrum of graphite paper after discharging to 1.6V

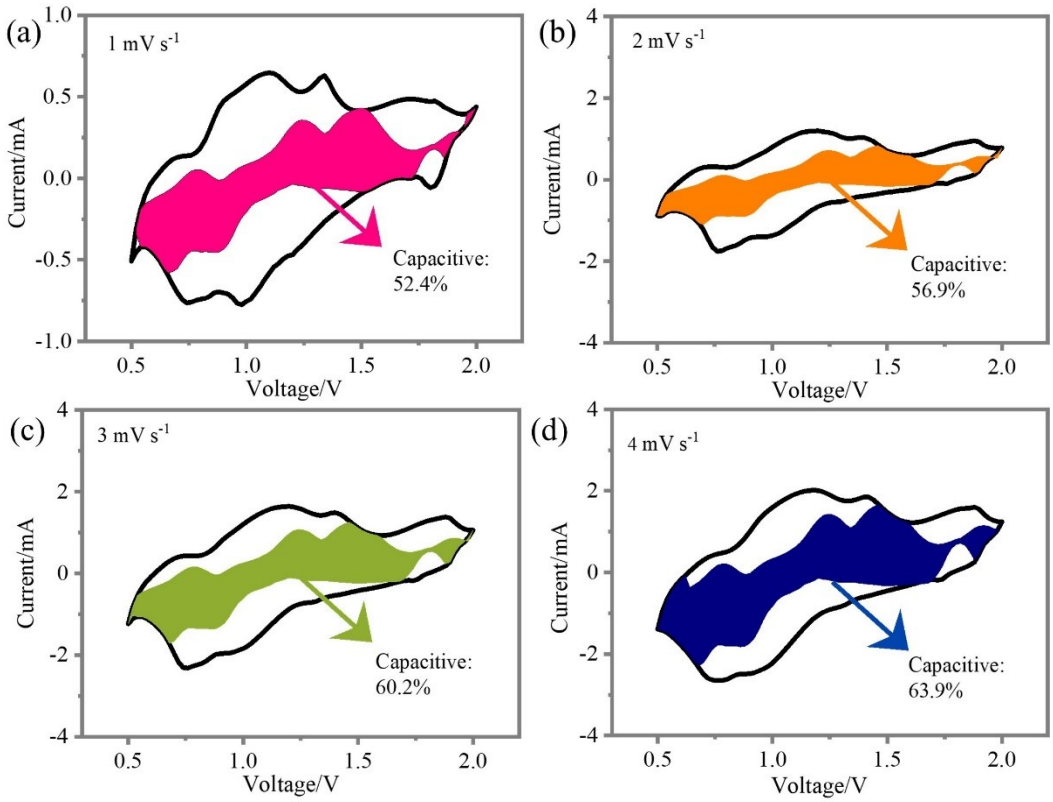

Figure S20 Separations of storage contribution from the capacitance and diffusion-controlled process at 1-4 mV s^{-1}.

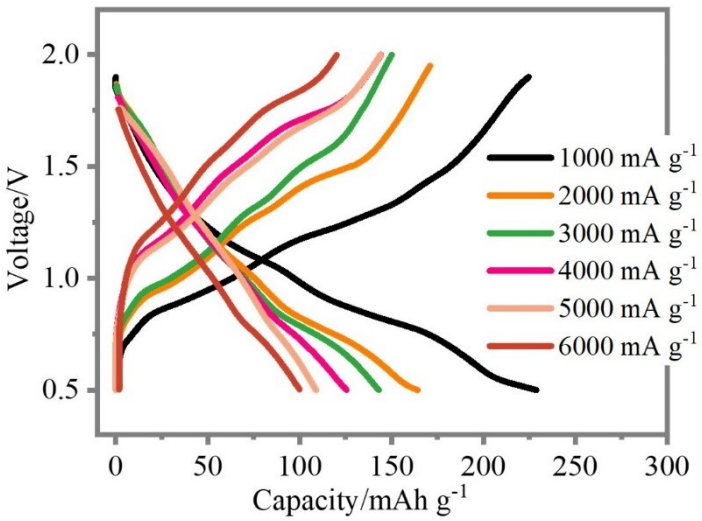

Figure S21 Galvanostatic charging/discharging profiles at various current density from 1000 to 6000 mA g^{-1}

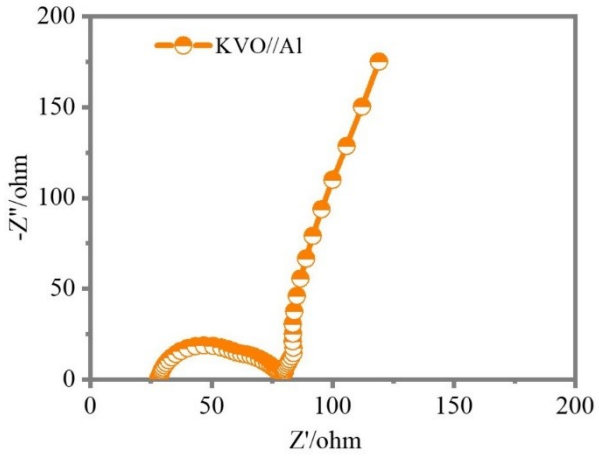

Figure S22 Nyquist plot of KVO//Al AAIB.

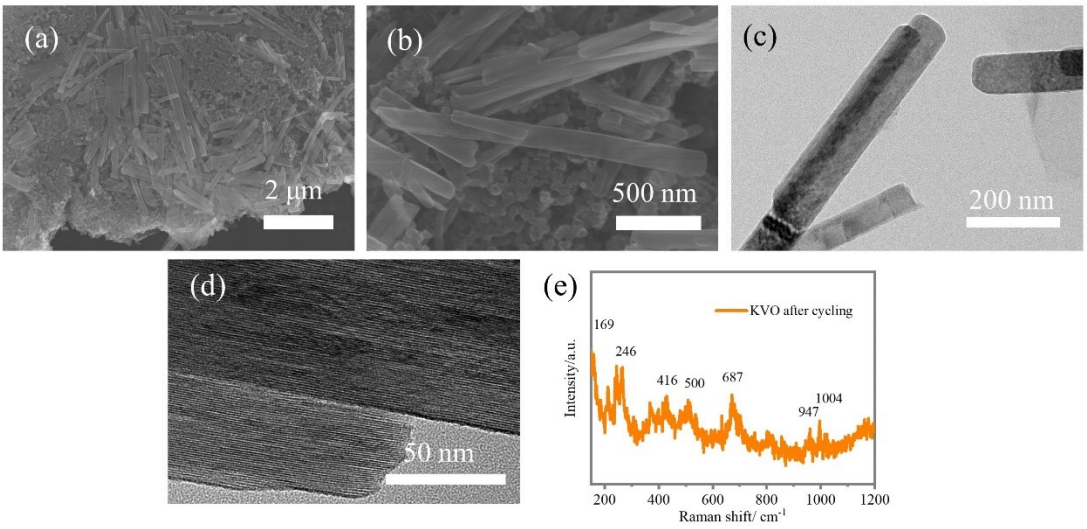

Figure S23 (a-b) SEM images, (c-d) TEM images, and (e) Raman spectrum of KVO after cycling.

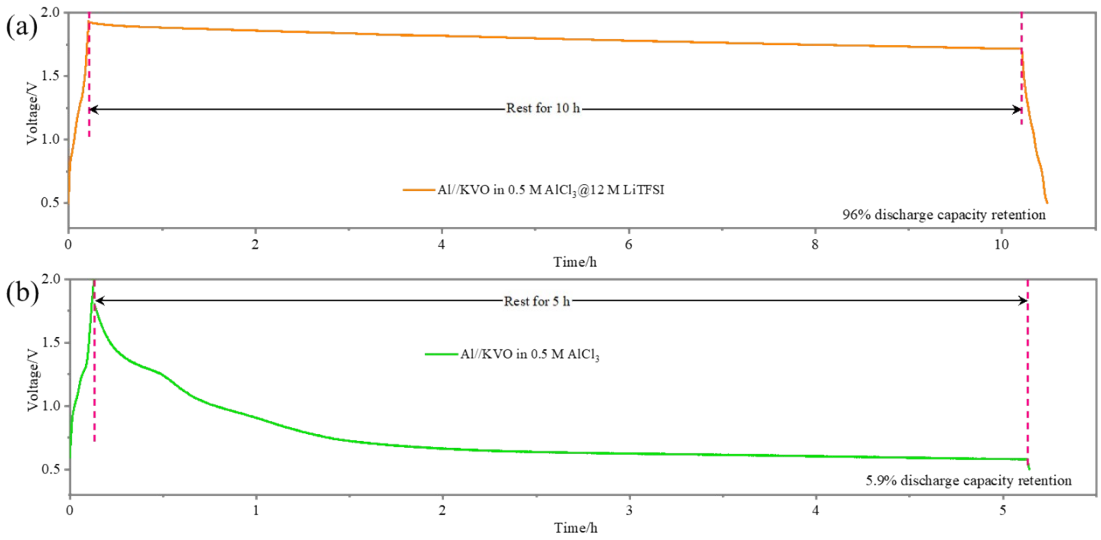

Figure S24 Self-discharge curves of Al//KVO batteries with different electrolytes.

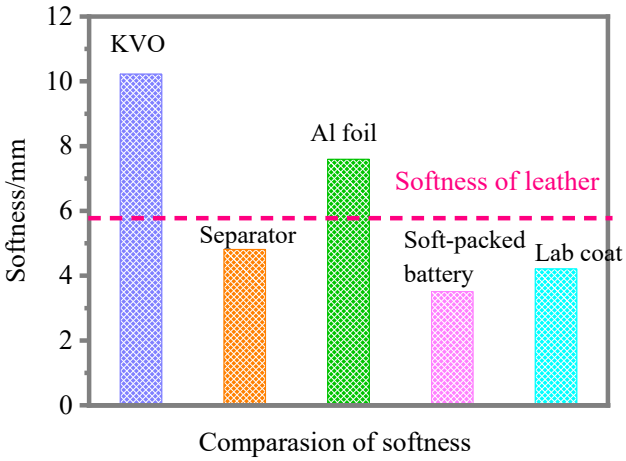

Figure S25 Softness evaluation of the battery

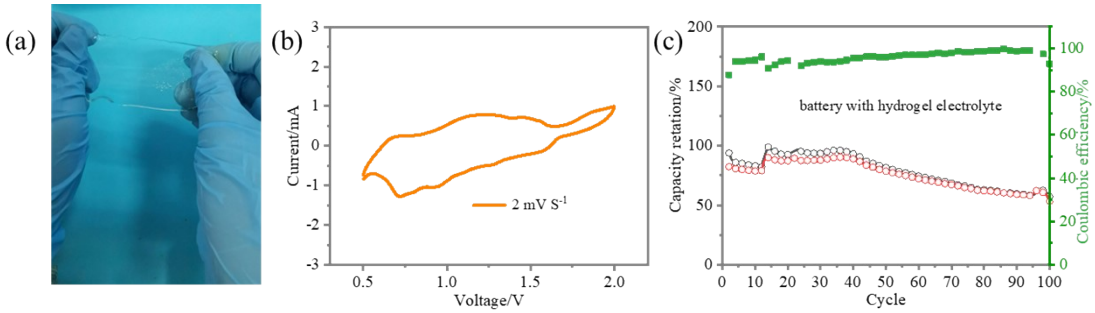

Figure S26 (a) optical image of PAA hydrogel, (b) CV curve, and (c) cycling stability of KVO//Al with PAA-based electrolyte

[1] L. Deng, X. Niu, G. Ma, Z. Yang, L. Zeng, Y. Zhu, L. Guo, *Adv. Funct. Mater.* **2018,** *28*, 1800670.